Computers, Materials & Continua

Tech Science Press

https://doi.org/10.32604/cmc.2026.077724

ARTICLE

Thermodynamic and Thermoelastic Properties of SiSn: Data Mining-Based Searches and High Compression Effect

Rabie Mezouar[1,2], Fouad Okba[3], Dejan Zagorac[4,5,*], Salah Daoud[2] and Abdelfateh Benmakhlouf[2]

[1]Institute of Optics and Precision Mechanics, Ferhat Abbas Setif 1 University, Setif, Algeria
[2]Laboratory of Materials and Electronic Systems, Faculty of Sciences and Technology, University Mohamed El Bachir El Ibrahimi of Bordj Bou Arreridj, Bordj Bou Arreridj, Algeria
[3]Architecture Department, Institute of Architecture and Earth Sciences, Ferhat Abbas Setif 1 University, Setif, Algeria
[4]Centre of Excellence "CextremeLab", Centre for Synthesis, Processing, and Characterization of Materials for Application in Extreme Conditions, University of Belgrade, Belgrade, Serbia
[5]Department of Material Science, Vinča Institute of Nuclear Sciences—National Institute of the Republic of Serbia, University of Belgrade, Belgrade, Serbia

*Corresponding Author: Dejan Zagorac. Email: dzagorac@vin.bg.ac.rs

Received: 16 December 2025; Accepted: 09 April 2026; Published: 08 May 2026

ABSTRACT: The compression effects on the thermoelastic and thermodynamic properties of cubic zincblende silicon–tin alloy (SiSn) were explored using a multi-methodological approach, deploying data mining methods, theoretical equation-of-state parameters, and the Quasi-Harmonic Debye Model. We analyze the relative volume, isothermal bulk modulus, thermal expansion coefficient, Debye temperature, sound velocity, and microhardness of the SiSn compound under pressures up to 8 GPa. The study commences with the data mining-based searches for a structural model and continues with an analysis of the pressure dependence of the relative volume using the Vinet equation of state, followed by an investigation of the bulk modulus and other related thermoelastic properties. Moreover, the variation of microhardness with temperature is predicted, demonstrating a patent progressive decline as the temperature rises from 0 to 800 K. The thermodynamic properties of the SiSn compound have been explored using the quasi-harmonic Debye model in temperatures ranging from 0 to 800 K and pressures ranging from 0 to 8 GPa, respectively. In addition to the information not found in the literature and offered by this study, our work also establishes a simplified model that can predict the evolution of microhardness as a function of temperature, firstly for the SiSn compound, and perhaps can extend to group-IV semiconductors.

KEYWORDS: Silicon-tin; SiSn; equation of state; high pressure; thermo-elastic properties; data mining; microhardness

PACS Classification: 61.72.Tt;65.40.−b;62.50.−p; 62.20.−x

1 Introduction

Group-IV semiconducting alloys possess immense potential for next-generation Si-based electronic and photonic device applications [1]. To investigate the thermodynamic properties, structural parameters, and elastic constants of cubic zinc-blende SiSn, Zhang et al. [1] employed first-principles calculations based on density functional theory (DFT). In addition, using density functional perturbation theory (DFPT), they attempted to accurately scrutinise the influence of high pressure on the dynamical properties (phonon frequencies) of the ordered $Si_{0.5}Sn_{0.5}$ alloy in the same phase.

By applying the empirical pseudo-potential method (EPM), Amrane et al. [2] endeavored to explore the electronic characteristics of SiSn and GeSn semiconducting materials, while Zaoui et al. [3] analyzed their optical and electronic properties.

The presence of a band gap is one of the most typical properties of semiconductors [4]. For SiSn, the indirect transition occurs at 0.91 eV, and for GeSn at 0.56 eV. The direct transition, on the other hand, appears at 1.14 eV for SiSn and 0.063 eV for GeSn, respectively [3].

By integrating DFT with electron–phonon coupling theory, Huang et al. [5] demonstrated that silicon–tin (SiSn) alloys exhibit remarkable thermoelectric performance at high temperatures. Moreover, Yalameha and Nourbakhsh [6] investigated the effects of germanium (Ge) concentration and hydrostatic pressure on the topological phase of $SnSi_{1-x}Ge_x$ alloys through first-principle calculations. They concluded that all $SnSi_{1-x}Ge_x$ compositions are dynamically stable.

Using a plane-wave pseudopotential approach within the DFT framework, Elias [7] examined the structural, elastic, electronic, optical, as well as thermodynamic properties of ordered SiGe, SiSn, and GeSn alloys crystallizing in the zinc-blende structure. Likewise, Zhang et al. [8] drew upon DFT and DFPT within the local density approximation (LDA) to analyse the structural stability, dynamical properties, elastic constants, and thermodynamic behavior of SiGe, SiSn, and GeSn materials. They concluded, amongst other things, that SiGe exhibits the highest structural stability among them.

A noteworthy experimental contribution was made by Tonkikh et al. [9]. They successfully synthesized the zinc-blende phase of SnSin anocrystals by virtue of molecular beam epitaxy within a Si matrix, subsequently confirmed by electron microscopy observations.

2 Theoretical Methods

The SiSn compound was investigated using a multi-methodological approach [10]. A multi-methodological approach employs two or more distinct research methods (qualitative, quantitative, or a combination) within one study or program to achieve a deeper understanding, offset the limitations of individual methods, and enhance the strength of conclusions by examining a problem from various perspectives. It frequently requires merging various approaches to grasp different aspects of a phenomenon, yielding more profound insights than a single method could achieve alone, resulting in enhanced validation and more comprehensive outcomes.

In this study, we have used three methods of investigation: Data Mining (DM), Equation of State (EOS), and Quasi-Harmonic Debye Model (QHDM). For DM based searches, we have used the Web of Science (WoS) database and Inorganic Crystal Structure Database (ICSD) [11,12]. To examine the behavior of the thermoelastic properties of the SiSn material under hydrostatic pressure, we applied the third-order Vinet equation of state (EOS) model [13,14]. Finally, the thermodynamic properties were computed using the QHMD approach and the GIBBS code [15].

3 Results and Discussion

3.1 Data Mining-Based Searches for Qualitative Data

First, we have explored the WoS database searching for the SiSn compound. Recent theoretical and experimental work has been found dealing with structural, elastic, and thermodynamic properties [1,8], growth of SiSn alloys on Si or GeSn-buffered Si(100), SiSn semiconductors and heterostructures, combinatorial thin films, structural and optical characterization of SiSn alloys grown by molecular beam

epitaxy, polycrystalline SiSn alloys grown on insulating layers, compositional dependence of the band-gap of Ge-Si-Sn alloys, novel avalanche photodiode (APD) that utilizes the SiSn-on-Si, SiSn, and SiOC composites [1,8,16–20].

In the next step, a data mining-based search of the ICSD Database was conducted based on similarities to known crystallographic structures. The ICSD is the most complete database for inorganic crystal structures (including minerals, metals, and alloys) with more than 300,000 structures [11,12]. This approach has been effective in identifying additional structural modifications in a variety of chemical systems [21]. Consistent with its previous successful applications, the well-established KDD (knowledge discovery in databases) methodology, comprising selection, preprocessing, transformation, and evaluation, was employed [22–24].

As a result, we find a total of 321 crystal structures containing Si and Sn atoms. Most of those structures come from experimental observations (205 inorganic structures), a great amount from experimental Metal-Organic Framework (108 MOF structures), and only eight theoretical structures (Fig. 1). Out of these eight theoretical structures, four of them contain additional Mg, Ca, O, and N atoms [25–28].

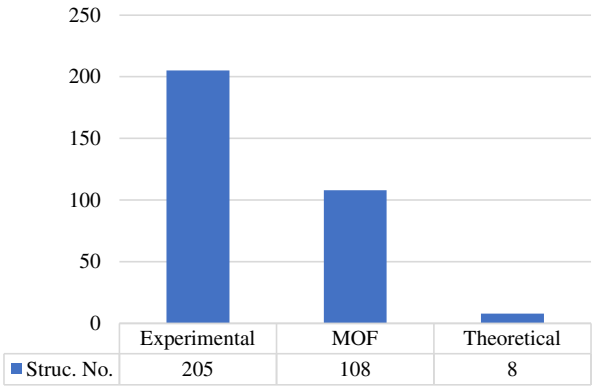

Figure 1: Short diagram of the results of data mining-based searches in the ICSD database, finally resulting in 8 theoretical structure candidates containing Si and Sn atoms.

From the remaining four theoretical strcutures in the binary SiSn chemical system, only two modifications were fond in the targeted SiSn compound: equilibrium cubic form, appearing in thezinc-blende (B3) structure and crystallizing in the cubic *F43m* (no. 216) space group, with the Si atom in the 4a (0, 0,0) and the Sn atom in the 4c (0.25, 0.25, 0.25) Wyckoff position (Fig. 2a) [1], and theoretical tetragonal model, crystallizing in the *P4/ncc* (no. 130) space group (Fig. 2b) [29]. An additional two structures were found theoretically in the $Si_{64}Sn$ chemical system, appearing in the cubic *P-43m* (no. 215) and rhombohedral *R3mR* (no. 160) space groups [30].

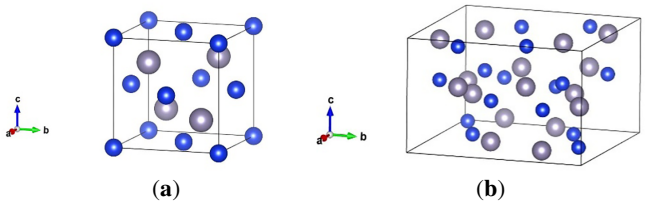

Figure 2: Visualization of SiSn modifications found after data mining in the ICSD: (**a**) equilibrium cubic form, appearing in the zinc-blende (B3) structure and crystallizing in the *F43m* (no. 216) space group [1], (**b**) theoretical tetragonal model, crystallizing in the *P4/ncc* (no. 130) space group [24]. Grey and blue spheres denote Sn and Si atoms, respectively.

Notably, there is a marked scarcity of published literature and documented crystal structures in major databases regarding this system. This lack of foundational data underscores the necessity for further research to enable robust data mining and machine-learning analysis. Consequently, this study represents a pioneering effort in the characterization of the SiSn system, establishing a framework for future investigations.

An analysis of the eight potential crystal structures within the ICSD database reveals that the majority consist of non-stoichiometric or non-equilibrium phases. Conventionally, the cubic diamond phase—specifically the cubic zinc-blende (B3) phase for binary compounds—represents the most prevalent and thermodynamically stable equilibrium structure for Group-IV semiconductors. In the present study, we focus primarily on the pressure dependence of the thermoelastic properties of the cubic zinc-blende (B3) SiSn compound, utilizing equilibrium structural parameters reported in the literature [1]. Furthermore, we predict the temperature dependence of microhardness using thermodynamic data also drawn from the same source [1]. Our work also offers a simplified model that can predict the evolution of microhardness with temperature. While this study focuses primarily on the SiSn compound, the findings may be extended to other Group-IV semiconductors.

3.2 Pressure Dependence of the Relative Volume

In order to investigate structural properties and later derived mechanical properties under compression, corresponding volumes of the zinc-blende type modification in the SiSn chemical system at pressures up to 8 GPa were analyzed. To examine the behavior of the structural parameters of the (B3) SiSn under hydrostatic pressure, we applied the third-order Vinet equation of state (EOS) model [13]. This equation relates the pressure p to the relative volume V/V_0 through the following expression [13]:

$$P(V) = 3B_0 \left(\frac{1-x}{x^2}\right) \exp\left[\eta(1-x)\right] \tag{1}$$

where, $x = (V/V_0)^{1/3}$, and $\eta = 3(B_0' - 1)/2$.

Hence, B_0 denotes the equilibrium bulk modulus, V refers to the volume of the unit cell at various pressures, V_0 signifies the equilibrium volume, whereas B_0' is the equilibrium pressure derivative of B.

Zhang et al. [1] maintain that the binary compound SiSn may crystallize in the zinc-blende lattice, as demonstrated by the known material 3C–SiC. Based on the theoretical values of the lattice constant (a_0 = 5.81 Å), the bulk modulus (B_0 = 72.47 GPa) and its pressure derivative (B_0' = 4.40) [1], the variation of the relative volume V/V_0 with pressure for cubic zinc-blende SiSn material is listed in Table 1.

Table 1: Relative volume V/V_0 vs. pressure for SiSn material.

***p* (GPa)**	**0**	**1.0**	**2.0**	**3.0**	**4.0**	**5.0**	**6.0**	**7.0**	**8.0**
V/V_0	1.00	0.99	0.97	0.96	0.95	0.94	0.93	0.92	0.91

The relative volume of the SiSn material is observed to decrease steadily with increasing pressure up to 8 GPa. It is known from the literature on other chemical systems that volume decreases with increasing pressure and can even cause defects and phase transitions [31–34]. In the case of SiSn, as the pressure rises from 0 to 8 GPa, the V/V_0 of SiSn decreases from 1 to 0.913. These results are essential for a deeper understanding of the structural characteristics of the SiSn compound.

3.3 Pressure Dependence of the Bulk Modulus

If one wants to investigate high pressure effect of inorganic material, it is of vital importance to investigate the resistance to volume change under pressure, represented by the bulk modulus. The bulk modulus B can be defined as the pressure p divided by the strain ε [35], or, in other words is defined as the derivative of pressure p with respect to volume V [36]. Within the framework of the third-order Vinet equation of state (EoS) [13], the isothermal bulk modulus B can be evaluated under extreme pressure conditions as follows [13,37]:

$$B(p) = B_0 x^{-2}\left[2 + (\eta - 1)x - \eta x^2\right]\exp\{\eta(1-x)\} \tag{2}$$

hence, $x = (V/V_0)^{1/3}$, and $\eta = 3(B_0' - 1)/2$.

The variations of B for SiSn vs. the pressure are listed in Table 2. As the pressure varied from 0 to 8 GPa, the bulk modulus of SiSn changed from 72.47 to 105.48 GPa. This is in agreement with other binary compounds, e.g., cubic copper iodide [31] and $BaTiO_3$ compound [38], where the bulk modulus increases with the increase of pressure.

Table 2: Bulk modulus vs. pressure for cubic (B3) SiSn material.

p (GPa)	0	1.0	2.0	3.0	4.0	5.0	6.0	7.0	8.0
V/V_0	72.5	76.8	81.1	85.3	89.5	93.5	97.5	101.5	105.5

3.4 Pressure Dependence of the Thermal Expansion Coefficient

Understanding the thermal expansion coefficient is indispensable for crystal growth, heterojunction formation [39], and the design of semiconductor devices [40]. The thermal expansion behavior of the SiSn compound under high pressure is examined under this heading. The volumetric thermal expansion coefficient can be expressed as a function of pressure as follows [41,42]:

$$\alpha(p) = \alpha_0\left(\frac{B_T(p)}{B_0}\right)^{-1}\left(\frac{V(p)}{V_0}\right)^{-1} \tag{3}$$

α_0, B_0, and V_0 denote the equilibrium thermal expansion coefficient, the equilibrium bulk modulus, and the equilibrium volume, respectively.

Eq. (4) can be derived by replacing the expression of Eq. (2) for the isothermal bulk modulus B into Eq. (3), as shown below:

$$\alpha(p) = \alpha_0 x^{-1}\left[2 + (\eta - 1)x - \eta x^2\right]^{-1}\exp\{-\eta(1-x)\} \tag{4}$$

where $x = (V/V_0)^{1/3}$, $\eta = 3(B_0' - 1)/2$, and α_0 is the equilibrium thermal expansion coefficient.

With regard to the average value $\alpha_{L0} = 0.5 \times (4.3 + 5.3) \times 10^{-6}\ K^{-1} = 4.8 \times 10^{-6}\ K^{-1}$ obtained from that ($4.3 \times 10^{-6}\ K^{-1}$) for Si and that ($5.3 \times 10^{-6}\ K^{-1}$) for Sn, respectively [39]. The curve of the linear thermal expansion coefficient α_L for SiSn material vs. the pressure p acquired in this work is plotted in Fig. 3. As the pressure varied from 0 to 8 GPa, α_L of SiSn material changes from 4.8 to $3.61 \times 10^{-6}\ K^{-1}$.

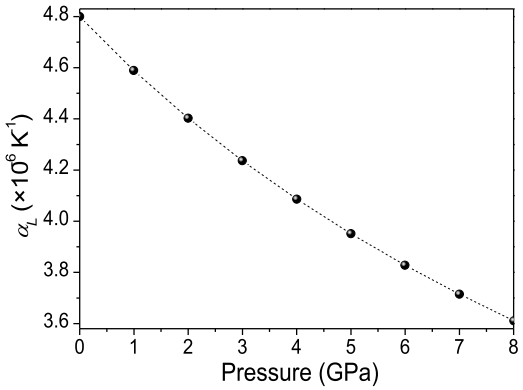

Figure 3: Linear thermal expansion coefficient α_L vs. pressure of cubic zinc-blende SiSn material.

3.5 Debye Temperature and the Sound Velocity

A simplified model that correlates the Debye temperature (θ_D) with the mass density (ρ) and the Grüneisen parameter (γ) is expressed by the following equation [43–45]:

$$\theta_D = \theta_{D0}\,(\rho/\rho_0)^{\gamma} \tag{5}$$

here, θ_{D0} and ρ_0 denote the equilibrium Debye temperature and mass density, respectively. The Vashchenko–Zubarev Grüneisen parameter (γ), the bulk modulus (B), and the pressure (p) are related through the following expression [46]:

$$\gamma_{V-Z}\,(p) = \left(\frac{1}{2}B' + \frac{2}{9}\left(\frac{p}{\mathrm{B}}\right) - \frac{5}{6}\right) / \left(1 - \frac{4p}{3\mathrm{B}}\right) \tag{6}$$

It is crucial to point out that B' is the pressure derivative of the isothermal bulk modulus. It is given as follows [47]:

$$B'\,(p) = \frac{1}{3}\left[\frac{x\,(1-\eta) + 2\eta x^2}{1 + (\eta x + 1)\,(1-x)} + (\eta\, x + 2)\right] \tag{7}$$

where p is the pressure, $x = (V/V_0)^{1/3}$, and $\eta = 3\,(B_0' - 1)\,/2$.

Considering the equilibrium theoretical value of the Debye temperature (θ_{D0} = 331.5 K) [1] and substituting the expressions of Eqs. (2) and (7) into Eq. (6), followed by inserting the resulting relation into Eq. (5), the pressure-dependent variation of the θ_D for the SiSn crystal was determined, as depicted in Fig. 4. The results indicate that the θ_D of SiSn exhibits a monotonic increase with rising pressure. A comparable qualitative trend of θ_{D} variation has been documented for the SiSn compound [1], for the binary compound calcium oxide (CaO) up to 65.2 GPa [44], for cubic gallium antimonide (GaSb) up to 6.2 GPa [45], for OsB crystal up to 90 GPa [48], for the thermoelectric materials SrCuP and SrCuSb [49], and for several other materials [50,51]. As the applied pressure increases from 0 to 8 GPa, the θ_D of SiSn increases from 331.5 to 371.8 K.

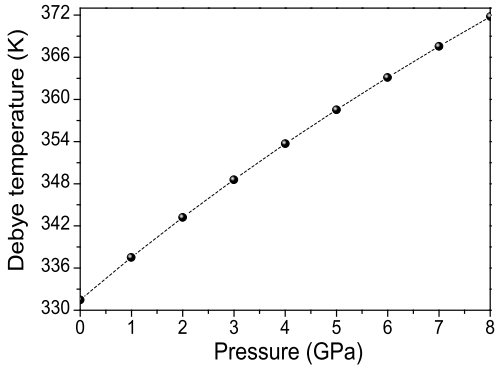

Figure 4: Debye temperature θ_D vs. pressure for SiSn material.

To determine the average sound velocity (v_m) from the Debye temperature θ_D, the following relation can be employed:

$$v_m = k_B\theta_D/\sqrt[3]{6\pi^2\hbar^3N/V} \tag{8}$$

Herein $\hbar = h/2\pi$, h refers to the Planck constant, k_B is the Boltzmann constant, and N/V is used to symbolize the concentration of atoms.

Table 3 lists the pressure dependence of the average sound velocity (v_m) for the SiSn crystal. It is evident from the figure that v_m of SiSn increases nonlinearly with increasing pressure up to 8 GPa. A similar trend has been reported for several materials, including the calcium oxide (CaO) compound [44], cubic anti-ReO_3-type Cu_3N material [52,53], orthorhombic Hg_2GeO_4 mineral material up to 10 GPa [54], and for superconductor $CuNNi_3$ ternary material under pressureup to 20 GPa [55].

Table 3: Sound velocity v_m vs. pressure p up to 8 GPa for SiSn crystal.

p (GPa)	0	1.0	2.0	3.0	4.0	5.0	6.0	7.0	8.0
v_m (GPa)	3235	3280	3321	3360	3396	3430	3462	3492	3521

3.6 Pressure Dependence of the Microhardness

Several empirical formulas are commonly employed to estimate hardness from elastic constants. The Vickers hardness, Hv, can be evaluated from the elastic moduli using the following expression [56,57]:

$$H_V = 0.92\,k^{1.137}G^{0.708} \tag{9}$$

The k in the equation above designates the Pugh's ratio ($k = G/B$).

Concerning the numerical values of the bulk modulus (B_0 = 72.5 GPa) and that of the shear modulus (G_0 = 42.9 GPa) [1], the value of Hv_0 for the SiSn crystal is 7.25 GPa. Based on the evolution of the Debye temperature θ_D with both temperature and pressure, Zhang et al. [1] conclude that the SiSn crystal maintains its hardness under elevated temperature and pressure conditions. Mukhanov et al. [58] undertakings have been devoted to developing a simplified model describing the pressure dependence of hardness. The model proposed by Mukhanov et al. [58] is expressed as follows: $H(p) = C \times B(p)$, where $C = H(0)/B(0)$ [44,45]. Substituting the expression of Eq. (2) for the bulk modulus B into the previous expression to obtain Eq. (10) as follows:

$$H(p) = H_0 x^{-2}\left[2 + (\eta - 1)x - \eta x^2\right]\exp\{\eta(1-x)\} \tag{10}$$

where $x = (V/V_0)^{1/3}$, $\eta = 3(B_0' - 1)/2$, and H_0 is the equilibrium hardness.

Upon replacing the value of H_0 = 7.25 GPa in the previous equation, the pressure dependence of the microhardness H for the SiSn is listed in Table 4. This reveals that the H of the SiSn increases gradually alongside the rising pressure from 0 to 8 GPa. Similar qualitative behavior was reported for H for calcium oxide material [44], gallium antimonide semiconductor [45], nano materials (CdTe, ZnTe) [59], $InP_{1-x}Sb_x$ ternary alloys [60], and for both BP and BAs semiconductors [61].

Table 4: Microhardness H vs. pressure p up to 8 GPa for SiSn crystal.

p (GPa)	0	1.0	2.0	3.0	4.0	5.0	6.0	7.0	8.0
H (GPa)	7.25	7.68	8.11	8.53	8.95	9.36	9.76	10.16	10.55

3.7 Temperature Dependence of the Microhardness

In a previous work, Mukhanov et al. [62] have discussed an interesting approach introducing the Gibbs free energy of atomization to represent hardness-temperature dependence, which is applied to polycrystalline cubic zinc-blende boron nitride (c-BN) and monocrystalline diamond. Mukhanov et al. [58] proposed a second model introducing both plasticity coefficient α and bulk modulus B to express the Vickers hardness Hv as a function of temperature, which is given as:

$$\mathrm{H_V(T)} = \mathrm{H_V(300)}\,\frac{\alpha(\mathrm{T})\ \ \mathrm{B(T)}}{\alpha(300)\ \ \mathrm{B(300)}} \tag{11}$$

$\alpha(300)$ and $\alpha(\mathrm{T})$ above refer to the plasticity coefficients at 300 K and at given temperature T, respectively.

The influence of the temperature on plasticity (coefficient incorporated by the following empirical equation) [58]:

$$\alpha(\mathrm{T}) = \alpha(300)\left(1 - \mathrm{e}^{-\frac{2}{3}\frac{\mathrm{T_m}}{\mathrm{T}}}\right) \tag{12}$$

where $\mathrm{T_m}$ is the melting point.

Substituting the expression of Eq. (12) for $\alpha(\mathrm{T})$ into Eq. (11) in order to obtain Eq. (13) as follows:

$$\mathrm{H_V(T)} = \mathrm{H_V(300)}\,\frac{\mathrm{B(T)}}{\mathrm{B(300)}}\left(1 - \ \mathrm{e}^{-\frac{2}{3}\frac{\mathrm{T_m}}{\mathrm{T}}}\right) \tag{13}$$

Moreover, the temperature dependence of the bulk modulus (B_T) can be evaluated using the exponential model proposed by Bioud et al. [63], as expressed by the following relation [63,64]:

$$B(T) = B_0 - bTe^{-T_0/T} \tag{14}$$

Hence, B_0 is the absolute zero-temperature bulk modulus, while b and T_0 are two parameters depending on the compound under consideration.

Substituting the expression of Eq. (14) for $B(T)$ into Eq. (13) to obtain the simplified analytical model expressed in Eq. (15) as follows:

$$H_V(T) = H_{V0}\left(1 - \frac{b}{B_0} T e^{-\frac{T_0}{T}}\right) \times \left(1 - e^{-\frac{2}{3}\frac{T_m}{T}}\right) \quad (15)$$

Considering the zero-pressure bulk modulus $B(T)$ data reported by Zhang et al. [1], obtained using the quasi-harmonic Debye model [14], the fitted parameters for the SiSn crystal are B_0 = 70.2 GPa, $b = 2.11 \times 10^{-2}$ GPa/K, and T_0 = 192.1 K.

For materials with cubic crystal structures, the melting temperature (T_0, in K) and the elastic constant (C_{11}, in GPa) are correlated according to the following relation [65]:

$$T_m = [553\,\text{K} + (5.91\,\text{K/GPa})\, C_{11}\,(\text{GPa})] \pm 300\,\text{K} \quad (16)$$

Based on the numerical value of C_{11} = 118.5 GPa [1], the corresponding melting temperature (T_m) for the SiSn crystal is calculated to be 1253.34 ± 300 K. To the best of our knowledge, no reported data are available in the literature for the T_m of SiSn in the cubic zinc-blende phase. By substituting all the aforementioned parameters into the preceding equation (Eq. (16)), the temperature dependence of the microhardness (H) for the SiSn is presented in Table 5 and illustrated in Fig. 5, respectively.

Table 5: Microhardness H vs. temperature T up to 800 K for SiSn crystal.

T (K)	0	200	400	600	800
H (GPa)	7.25	6.90	5.82	4.68	3.77

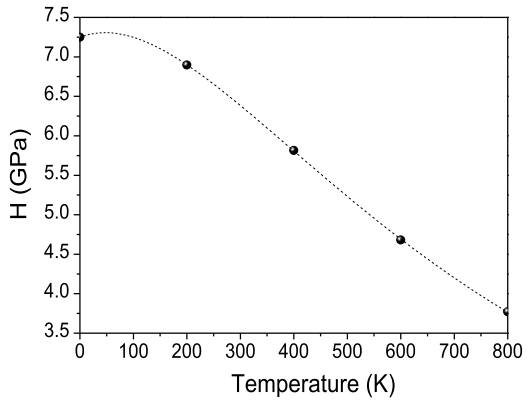

Figure 5: Microhardness H vs. temperature for SiSn crystal.

One major advantage of the proposed approach is its simplicity for the evaluation of the hardness of the SiSn compound, and it can extend to group-IV semiconductors. The results indicate that the microhardness (H) of the SiSn crystal decreases progressively as the temperature rises from 0 to 800 K. Altough, the similar qualitative behavior, which has been observed in other materials, including polycrystalline cubic boron subnitride (c-BN) [58], B_4C, SiC and Al_2O_3-based ceramics [58], single-crystal diamond [58], single-crystal ReB_2 material [58], cubic zinc-blende SiC material from 0 to 1000 K [66], LaB_6 single crystal [67], YB_6 single crystal [67], and for TiC single crystal [67]. Some differences have been noted on the trend of the curves $H(T)$ measured experimentally, such as the inflection points observed for LaB_6, YB_6 and TiC single crystals [67].

Above the inflection points, Chen et al. [67] found a high-accuracy in hardness measurement, and they proposed straight lines for the fitting of the hardness as a function of temperature. Furthermore, Mukhanov et al. [58] mentioned that the strong decrease of diamond hardness with temperature compared with other materials, perhaps, is due to the lower thermal expansion of diamond.

The effect of temperature on the microhardness (H) of the SiSn crystal is found to be more pronounced than that of pressure. Such pressure-temperature relations are also known in the literature on the TiNb alloys, where theoretical data are confirmed with experimental results [68].

4 Thermodynamic Properties

The GIBBS code [15] has been used to complete the calculations of the thermodynamic properties. The energy-volume (E-V) data inserted in the GIBBS code have been taken from Ref. [69]. The thermodynamic properties of the SiSn compound have been studied using the quasi-harmonic Debye model at temperatures ranging from 0 to 800 K and pressures ranging from 0 to 8 GPa, respectively. The variation of the Gibbs free energy G as a function of pressure at various temperatures (0, 300, 600 and 800 K) for SiSn material was illustrated in Fig. 6a, while the variation of G as a function of temperature T at different pressures (0, 2, 4, 6, and 8 GPa) was shown in Fig. 6b, respectively.

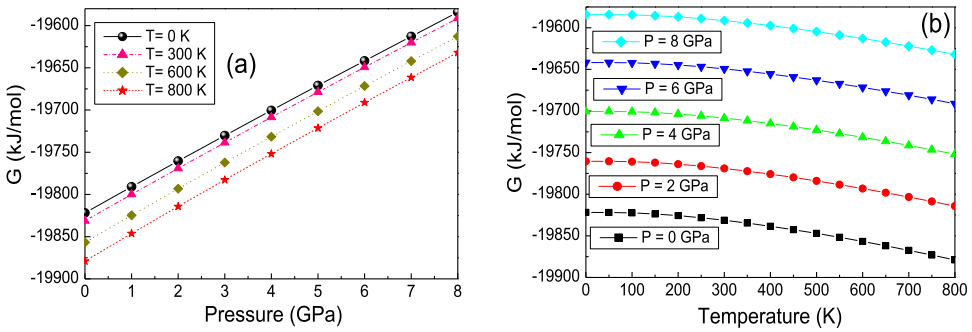

Figure 6: Relationships between Gibbs free energy G and pressure at various temperatures (**a**) and between G and temperature under different pressures (**b**) for SiSn.

It can be seen from Fig. 6a,b that the Gibbs free energy G of SiSn semiconducting material increases monotonically with increasing pressure, and inversely it decreases with increasing temperature. The decrease as a function of the increase of temperature is also observed for the Helmholtz free energy in similar group-IV alloys (SiGe, SiSn, and GeSn) [8].

Pressure and temperature dependencies of the unit cell volume V for SiSn semiconducting material are presented in Fig. 7a,b, respectively. Notice that V decreases with increasing pressure at all temperatures of interest. At temperatures of 0, 300, 600, and 800 K, the fits of our data regarding the volume V (in Å^3) for SiSn obey the following quadratic expressions, respectively:

$$V = 51.68 - 0.69p + 1.94 \times 10^{-2}p^2 \quad (17a)$$

$$V = 52.38 - 0.78p + 2.43 \times 10^{-2}p^2 \quad (17b)$$

$$V = 53.67 - 0.95p + 3.44 \times 10^{-2}p^2 \quad (17c)$$

$$V = 54.79 - 1.13p + 4.66 \times 10^{-2}p^2 \quad (17d)$$

where the pressure is expressed in GPa.

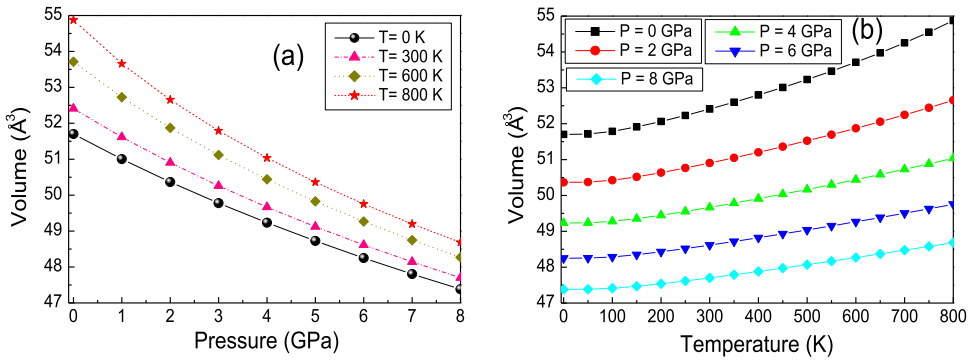

Figure 7: Plot between unit cell volume and pressure at various temperatures (**a**) and between unit cell volume and temperature at various pressures (**b**) for SiSn.

At various pressures (0, 2, 4, 6, and 8 GPa), the best fits of our data regarding the unit cell volume V (in Å^3) for SiSn as a function of temperature (in K) obey the following quadratic expressions, respectively:

$$V = 51.63 + 1.69 \times 10^{-3}\,\mathrm{T} + 2.96 \times 10^{-6}\mathrm{T}^2 \quad (18a)$$

$$V = 50.29 + 1.49 \times 10^{-3}\,\mathrm{T} + 1.86 \times 10^{-6}\,\mathrm{T}^2 \quad (18b)$$

$$V = 49.17 + 1.28 \times 10^{-3}\,\mathrm{T} + 1.36 \times 10^{-6}\,\mathrm{T}^2 \quad (18c)$$

$$V = 48.19 + 1.11 \times 10^{-3}\,\mathrm{T} + 1.09 \times 10^{-6}\,\mathrm{T}^2 \quad (18d)$$

$$V = 47.33 + 0.98 \times 10^{-3}\,\mathrm{T} + 0.93 \times 10^{-6}\,\mathrm{T}^2 \quad (18e)$$

The variation in the bulk modulus B_T as a function of pressure and temperature for SiSn semiconducting material is presented in Fig. 8a,b, respectively. It can be seen from these two figures that the bulk modulus B_T of SiSn increases monotonically with increasing pressure from 0 to 8 GPa, and inversely, it decreases with increasing temperature.

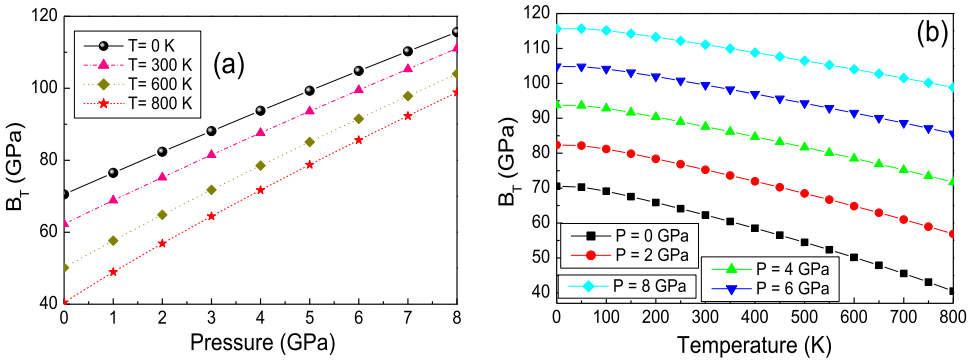

Figure 8: Bulk modulus B_T*vis* pressure at various temperatures (**a**) and plot between B_T and temperature at various pressures (**b**) for SiSn.

The increasing of B_T with increasing pressure and its decrease with increasing temperature were also observed for the cubic zinc-blende SiSn compound [1]. At $p = 0$ and $T = 0$ K, our calculation yielded a value of $B_T = 70.53$ GPa, which is in excellent agreement with the theoretical value (~71 GPa) reported by Zhang et al. [1] and obtained from the same approach, while at $p = 8$ GPa and $T = 0$ K, our calculation yielded

a value of B_T = 115.65 GPa, which is slightly higher than the theoretical value (~104.5 GPa) reported by Zhang et al. [1].

At temperatures of 0, 300, 600, and 800 K, the fits of our data on B_T for SiSn obey the following quadratic expressions, respectively:

$$B_T = 70.56 + 5.97p - 4.19 \times 10^{-2} p^2 \quad (19a)$$

$$B_T = 62.35 + 6.55p - 5.76 \times 10^{-2} p^2 \quad (19b)$$

$$B_T = 50.26 + 7.42p - 8.90 \times 10^{-2} p^2 \quad (19c)$$

$$B_T = 40.69 + 8.27p - 1.27 \times 10^{-2} p^2 \quad (19d)$$

where both the bulk modulus B_T and the pressure are expressed in GPa.

The variation in the Debye temperature θ_D for SiSn semiconducting material as a function of pressure at various temperatures and as a function of temperature at various pressures is presented in Fig. 9a,b, respectively. It can be seen from these two figures that the Debye temperature θ_D of SiSn increases monotonically with increasing pressure from 0 to 8 GPa, and inversely it decreases with increasing temperature.

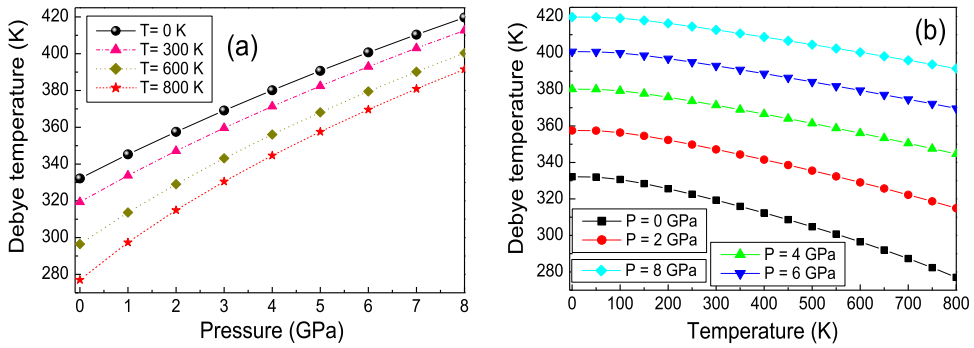

Figure 9: Plot between Debye temperature θ_D and pressure at various temperatures (**a**) and between θ_D and temperature at various pressures (**b**) for SiSn in cubic phase.

The increasing of θ_D with increasing pressure and the decrease in the Debye temperature θ_D with increasing temperature were also observed for cubic zinc-blende SiSn binary compound [1], and for $BaTiO_3$ compound [38]. At temperatures of 0, 300, 600, and 800 K, the fits of our data on θ_D for SiSn obey the following quadratic expressions, respectively:

$$\theta_D = 332.41 + 13.00p - 2.64 \times 10^{-1} p^2 \quad (20a)$$

$$\theta_D = 319.65 + 14.28p - 3.36 \times 10^{-1} p^2 \quad (20b)$$

$$\theta_D = 297.11 + 16.68p - 4.79 \times 10^{-1} p^2 \quad (20c)$$

$$\theta_D = 278.09 + 19.27p - 6.49 \times 10^{-1} p^2 \quad (20d)$$

where θ_D is expressed in K and p is in GPa.

The lines represent the least-square fits of θ_D (in K) at various pressures 0, 2, 4, 6, and 8 GPa, respectively:

$$\theta_D = 333.63 - 3.36 \times 10^{-2}\,\mathrm{T} - 4.67 \times 10^{-5}\,\mathrm{T}^2 \quad (21a)$$

$$\theta_D = 358.99 - 3.04 \times 10^{-2}\,\mathrm{T} - 3.16 \times 10^{-5}\,\mathrm{T}^2 \quad (21b)$$

$$\theta_D = 381.52 - 2.70 \times 10^{-2}\,\mathrm{T} - 2.48 \times 10^{-5}\,\mathrm{T}^2 \quad (21c)$$

$$\theta_D = 402.00 - 2.44 \times 10^{-2}\,\mathrm{T} - 2.10 \times 10^{-5}\,\mathrm{T}^2 \quad (21d)$$

$$\theta_D = 420.87 - 2.24 \times 10^{-2}\,\mathrm{T} - 1.87 \times 10^{-5}\,\mathrm{T}^2 \quad (21e)$$

At $p = 0$ and $T = 0$ K, our calculation yielded value of $\theta_D = 332.2$ K, which is in excellent agreement with theoretical value (~331.5 K) reported by Zhang et al. [1] and obtained from the same approach, while at $p = 8$ GPa and $T = 0$ K, our calculation yielded value of $\theta_D = 419.7$ K, slightly higher than the theoretical value (~396.5 K) reported by Zhang et al. [1].

5 Conclusion

This study investigated the pressure dependence of the relative volume, isothermal bulk modulus, thermal expansion coefficient, Debye temperature, sound velocity, and microhardness for the cubic zinc-blende SiSn crystal. Data mining-based searches have been performed in order to obtain qualitative data for further high-pressure investigations. As the applied pressure increases from 0 to 8 GPa, the relative volume of the SiSn decreases from 1 to 0.913, while the isothermal bulk modulus rises from 72.47 to 105.48 GPa. Hence, the linear thermal expansion coefficient decreases from 4.8 to 3.61×10^{-6} K^{-1}, whereas the Debye temperature increases from 331.5 to 371.8 K.

The thermodynamic properties of the SiSn compound have been studied using the GIBBS code and the quasi-harmonic Debye model in temperatures ranging from 0 to 800 K and pressures ranging from 0 to 8 GPa, respectively. The variation of the Gibbs free energy G as a function of pressure at various temperatures, 0, 300, 600, and 800 K, has been presented.

In addition, the microhardness (H) of the SiSn compound is calculated to be 7.25 GPa. The microhardness H of the SiSn decreases progressively from 7.25 to 3.77 GPa as the temperature increases from 0 to 800 K. It is worth mentioning that no experimental investigation has been reported on the SiSn compound. Therefore, the present results provide valuable theoretical predictions that may serve as a reference point for future experimental and computational studies on the SiSn compound. Furthermore, the simplified model established here can be useful to predict the dependence of the microhardness with temperature, initially used for the SiSn system, and offers significant potential for broader application across the Group-IV semiconductor family.

Acknowledgement: Not applicable.

Funding Statement: Dejan Zagorac acknowledges funding by the Ministry of Science, Technological Development, and Innovation of the Republic of Serbia through Contract No. 451-03-33/2026-03/200017.

Author Contributions: Rabie Mezouar: conceptualization, writing, formal analysis; Fouad Okba: review, visualization; Dejan Zagorac: methodology, writing, investigation, review; Salah Daoud: methodology, review, visualization; Abdelfateh Benmakhlouf: conceptualization, investigation, visualization. All authors reviewed and approved the final version of the manuscript.

Availability of Data and Materials: Data available on request from the authors. The data that support the findings of this study are available from the corresponding author, [Dejan Zagorac], upon reasonable request.

Ethics Approval: Not applicable, for studies not involving humans or animals.

Conflicts of Interest: The authors declare no conflicts of interest.

References

1. Zhang X, Ying C, Quan S, Shi G, Li Z. A first principles investigation on the structural, phonon, elastic and thermodynamic properties of the $Si_{0.5}Sn_{0.5}$ cubic alloy. Solid State Commun. 2012;152(11):955–9. doi:10.1016/j.ssc.2012.03.017.
2. Amrane N, Ait Abderrahmane S, Aourag H. Band structure calculation of GeSn and SiSn. Infrared Phys Technol. 1995;36(5):843–8. doi:10.1016/1350-4495(95)00019-U.
3. Zaoui A, Ferhat M, Certier M, Khelifa B, Aourag H. Optical properties of SiSn and GeSn. Infrared Phys Technol. 1996;37(4):483–8. doi:10.1016/1350-4495(95)00116-6.
4. Nabil B, Ouadha I, Youcef C, Louhibi-Fasla S, Samir B, Kamel H, et al. Structural, electronic and optical properties of $Sc_xGa_{1-x}P$ alloys an: ab initio study. Ann West Univ Timisoara Phys. 2021;63(1):111–28. doi:10.2478/awutp-2021-0008.
5. Huang S, Ning S, Xiong R. First-principles study of silicon-tin alloys as a high-temperature thermoelectric material. Materials. 2022;15(12):4107. doi:10.3390/ma15124107.
6. Yalameha S, Nourbakhsh Z. Influence of hydrostatic pressure and concentration of Ge on the topological band order of $SnSi_{1-x}Ge_x$ alloys. Mater Sci Eng B. 2022;281(2):115742. doi:10.1016/j.mseb.2022.115742.
7. Elias BH. Structural, electronic, elastic, optical and thermodynamical properties of zinc-blende SiGe, SiSn and GeSn from first principles. Adv Phys Theor Appl. 2013;25:82–91.
8. Zhang X, Ying C, Li Z, Shi G. First-principles calculations of structural stability, elastic, dynamical and thermodynamic properties of SiGe, SiSn. GeSn Superlattices Microstruct. 2012;52(3):459–69. doi:10.1016/j.spmi.2012.06.001.
9. Tonkikh A, Klavsyuk A, Zakharov N, Saletsky A, Werner P. SnSi nanocrystals of zinc-blende structure in a Si matrix. Nano Res. 2015;8(12):3905–11. doi:10.1007/s12274-015-0890-z.
10. Matović B, Maletaškić J, Maksimović V, Dimitrijević SP, Todorović B, Pejić M, et al. Multicomponent solid solution with pyrochlore structure. Boletín De La Soc Española De Cerámica Y Vidr. 2023;62(6):515–26. doi:10.1016/j.bsecv.2023.01.005.
11. Belsky A, Hellenbrandt M, Karen VL, Luksch P. New developments in the Inorganic Crystal Structure Database (ICSD): accessibility in support of materials research and design. Acta Crystallogr B. 2002;58(3):364–9. doi:10.1107/s0108768102006948.
12. Zagorac D, Müller H, Ruehl S, Zagorac J, Rehme S. Recent developments in the Inorganic Crystal Structure Database: theoretical crystal structure data and related features. J Appl Crystallogr. 2019;52(5):918–25. doi:10.1107/S160057671900997X.
13. Vinet P, Rose JH, Ferrante J, Smith JR. Universal features of the equation of state of solids. J Phys Condens Matter. 1989;1(11):1941–63. doi:10.1088/0953-8984/1/11/002.
14. Jeanloz R. Universal equation of state. Phys Rev B. 1988;38(1):805–7. doi:10.1103/physrevb.38.805.
15. Otero-de-la-Roza A, Abbasi-Pérez D, Luaña V. Gibbs2: a new version of the quasiharmonic model code. II. Models for solid-state thermodynamics, features and implementation. Comput Phys Commun. 2011;182(10):2232–48. doi:10.1016/j.cpc.2011.05.009.
16. Tolle J, Chizmeshya AVG, Fang YY, Kouvetakis J, D'Costa VR, Hu CW, et al. Low temperature chemical vapor deposition of Si-based compounds via $SiH_3SiH_2SiH_3$: metastable SiSn/GeSn/Si(100) heteroepitaxial structures. Appl Phys Lett. 2006;89(23):231924. doi:10.1063/1.2403903.
17. Kouvetakis J, Chizmeshya AVG. New classes of Si-based photonic materials and device architectures via designer molecular routes. J Mater Chem. 2007;17(17):1649–55. doi:10.1039/b618416b.
18. Timofeev VA, Nikiforov AI, Tuktamyshev AR, Mashanov VI, Loshkarev ID, Bloshkin AA, et al. Pseudomorphic GeSiSn, SiSn and Ge layers in strained heterostructures. Nanotechnol. 2018;29(15):154002. doi:10.1088/1361-6528/aaac45.
19. Lin H, Chen R, Lu W, Huo Y, Kamins TI, Harris JS. Structural and optical characterization of $Si_xGe_{1-x-y}Sn_y$ alloys grown by molecular beam epitaxy. Appl Phys Lett. 2012;100(14):141908. doi:10.1063/1.3701732.
20. Do K, Park C, Hwang J, Kim S, Jung Y, Lee SH, et al. Covalent-assisted seeding of Si nanoparticles into a dual-matrix design toward advanced Si-based Li-ion batteries. J Mater Chem A. 2024;12(18):11062–74. doi:10.1039/d3ta07989a.

21. Sultania M, Schön JC, Fischer D, Jansen M. Investigation of structural relations among the compounds in the ICSD using geometry based comparison techniques. Struct Chem. 2012;23(4):1121–9. doi:10.1007/s11224-012-0008-0.
22. Marbn S, Mariscal G, Segovi J. A data mining & knowledge discovery process model. In: Data mining and knowledge discovery in real life applications. Rijeka, Croatia: IntechOpen; 2009. doi:10.5772/6438.
23. Škundrić T, Zagorac D, Schön J, Pejić M, Matović B. Crystal structure prediction of the novel Cr_2SiN_4 compound via global optimization, data mining, and the PCAE method. Crystals. 2021;11(8):891. doi:10.3390/cryst11080891.
24. Pejić M, Zimmermann DD, Zagorac D, Fonović M, Zagorac J, Schön JC, et al. Structural exploration of holmium fluoride selenide (HoFSe): theory and experiment. J Phys Chem Solids. 2026;208(4):113000. doi:10.1016/j.jpcs.2025.113000.
25. Kim CE, Soon A, Stampfl C. Unraveling the origins of conduction band valley degeneracies in $Mg_2Si_{1-x}Sn_x$ thermoelectrics. Phys Chem Chem Phys. 2016;18(2):939–46. doi:10.1039/c5cp06163f.
26. Tian M, Wei C, Zhang J, Wang J, Yang R. Electronic, optical, and water solubility properties of two-dimensional layered $SnSi_2N_4$ from first principles. Phys Rev B. 2021;103(19):195305. doi:10.1103/physrevb.103.195305.
27. Eremin NN, Urusov VS, Rusakov VS, Yakubovich OV. Precision X-ray diffraction and Mössbauer studies and computer simulation of the structure and properties of malayaite $CaSnOSiO_4$. Crystallogr Rep. 2002;47(5):759–67. doi:10.1134/1.1509390.
28. Yao W, Hu S, Jia F, Reimers JR, Wang Y, Singh DJ, et al. Lattice strain and band overlap of the thermoelectric composite $Mg_2Si_{1-x}Sn_x$. Phys Rev B. 2022;106(10):104303. doi:10.1103/physrevb.106.104303.
29. Si Z, Chai C, Zhang W, Song Y, Yang Y. Theoretical investigation of group-IV binary compounds in the *P*4/*ncc* phase. Results Phys. 2021;26(2):104349. doi:10.1016/j.rinp.2021.104349.
30. Sluydts M, Pieters M, Vanhellemont J, Van Speybroeck V, Cottenier S. High-throughput screening of extrinsic point defect properties in Si and Ge: database and applications. Chem Mater. 2017;29(3):975–84. doi:10.1021/acs.chemmater.6b03368.
31. Bioud N, Kassali K, Sun XW, Song T, Khenata R, Bin-Omran S. High-pressure phase transition and thermodynamic properties from first-principles calculations: application to cubic copper iodide. Mater Chem Phys. 2018;203:362–73. doi:10.1016/j.matchemphys.2017.10.016.
32. Zagorac D, Zagorac J, Djukic MB, Jordanov D, Matović B. Theoretical study of AlN mechanical behaviour under high pressure regime. Theor Appl Fract Mech. 2019;103:102289. doi:10.1016/j.tafmec.2019.102289.
33. Matović B, Urbanovich V, Babu GCSM, Maletaskic J, Lukovic A, Ercic J, et al. Sintering and characterization of additive-free B_4C/SiC_w composites using high-pressure techniques. Int J Appl Ceram Technol. 2025;22(6):e70036. doi:10.1111/ijac.70036.
34. Čančarević ŽP, Schön JC, Jansen M. Stability of alkali metal halide polymorphs as a function of pressure. Chem Asian J. 2008;3(3):561–72. doi:10.1002/asia.200700323.
35. Grzechnik A, Hakala BV, Kurig S, Walte N, Tsujino N, Kakizawa S, et al. Structures, phase stability, amorphization, and decomposition of V_6O_{13} at high pressures and temperatures: synthesis of rutile-related $V_{0.92}O_2$. Cryst Growth Des. 2024;24(13):5582–92. doi:10.1021/acs.cgd.4c00363.s001.
36. Zhang S, Cohen M. High-pressure phases of III–V zinc-blende semiconductors. Phys Rev B. 1987;35(14):7604–10. doi:10.1103/physrevb.35.7604.
37. Bioud N, Benchiheub N. Mechanical and thermal behavior of semiconducting cadmium oxide at high-pressure. Ann West Univ Timisoara Phys. 2024;66(1):142–56. doi:10.2478/awutp-2024-0009.
38. Ciftci YO, Durukan IK, Rani U, Kamlesh PK. Phase-dependent structural, optical, and thermodynamic behavior of $BaTiO_3$: insights from first-principles calculations. Comput Mater Contin. 2026;87(3):1–22. doi:10.32604/cmc.2026.078722.
39. Omar MS. Lattice thermal expansion for normal tetrahedral compound semiconductors. Mater Res Bull. 2007;42(2):319–26. doi:10.1016/j.materresbull.2006.05.031.
40. Omar MS. A modified model for calculating lattice thermal expansion of I_2–IV-VI_3 and I_3–V-VI_4 tetrahedral compounds. Mater Res Bull. 2007;42(5):961–6. doi:10.1016/j.materresbull.2006.08.008.
41. Fang ZH. Temperature dependence of volume thermal expansion for NaCl and KCl crystals. Phys B Condens Matter. 2005;357(3–4):433–8. doi:10.1016/j.physb.2004.12.010.

42. Goyal M. Melting temperature of metals under pressure. Chin J Phys. 2020;66(2020):453–60. doi:10.1016/j.cjph.2020.05.002.
43. Mohammed HB, AL-Faris SJ, Mahammed MA. Thermoelastic properties of CaO under high hydrostatic pressure using equations of state. Phys Lett A. 2025;546(3):130532. doi:10.1016/j.physleta.2025.130532.
44. Bioud N, Benchiheub N. Pressure effect on some physical properties of calcium oxide material. Chem Phys Impact. 2023;7:100342. doi:10.1016/j.chphi.2023.100342.
45. Benkara Mohammed N, Bioud N, Benchiheub N. Hydrostatic pressure response of semiconducting GaSb applying a semi-empirical approach. Comput Condens Matter. 2024;39(4):e00895. doi:10.1016/j.cocom.2024.e00895.
46. Vashchenko VY, Zubarev VN. Concerning the Grüneisen constant. Sov Phys Solid State. 1963;5:653–5.
47. Shah B. Study of the Grüneisen parameter of ZnO at high pressures. J Nano-Electron Phys. 2022;14(2):1–4. doi:10.21272/jnep.14(2).02020.
48. Chen HH, Li Z, Cheng Y, Bi Y, Cai LC. Thermodynamic properties of OsB under high temperature and high pressure. Phys B Condens Matter. 2011;406(17):3338–41. doi:10.1016/j.physb.2011.05.056.
49. Bioud N, Benchiheub N, Benamrani A, Ghebouli MA, Fatmi M, Alanazi FK, et al. Predicted thermodynamic structural and elastic properties of SrCuP and SrCuSb for thermoelectric applications. Sci Rep. 2025;15(1):4082. doi:10.1038/s41598-025-88280-1.
50. Wang C, Liang S, Cui J, Wang X, Wei Y. First-principles study of the mechanical and thermodynamic properties of Al_4W, Al_5W and $Al_{12}W$ under pressure. Vacuum. 2019;169:108844. doi:10.1016/j.vacuum.2019.108844.
51. Deng Y, Jia OH, Chen XR, Zhu J. Phase transition and elastic constants of CaO from first-principle calculations. Phys B Condens Matter. 2007;392(1–2):229–32. doi:10.1016/j.physb.2006.11.023.
52. Ghoohestani M, Karimipour M, Javdani Z. The effect of pressure on the physical properties of Cu_3N. Phys Scr. 2014;89(3):035801. doi:10.1088/0031-8949/89/03/035801.
53. Ghoohestani M, Karimipour M, Javdani Z. Reply to comment on 'The effect of pressure on the physical properties of Cu_3N'. Phys Scr. 2016;91(5):057002. doi:10.1088/0031-8949/91/5/057002.
54. Singh J, Errandonea D, Kanchana V, Vaitheeswaran G. Pressure-driven responses in Cd_2SiO_4 and Hg_2GeO_4 minerals: a comparative study. Crystals. 2024;14(6):538. doi:10.3390/cryst14060538.
55. Chen H, Lei X, Long J, Huang W. The elastic and thermodynamic properties of new antiperovskite-type superconductor $CuNNi_3$ under pressure. Mater Sci Semicond Process. 2014;27:207–11. doi:10.1016/j.mssp.2014.06.042.
56. Tian Y, Xu B, Zhao Z. Microscopic theory of hardness and design of novel superhard crystals. Int J Refract Met Hard Mater. 2012;33:93–106. doi:10.1016/j.ijrmhm.2012.02.021.
57. Adhikari V, Liu ZTY, Szymanski NJ, Khatri I, Gall D, Sarin P, et al. First-principles study of mechanical and magnetic properties of transition metal (M) nitrides in the cubic M_4N structure. J Phys Chem Solids. 2018;120(7):197–206. doi:10.1016/j.jpcs.2018.04.043.
58. Mukhanov VA, Kurakevych OO, Solozhenko VL. Hardness of materials at high temperature and high pressure. Philos Mag. 2009;89(25):2117–27. doi:10.1080/14786430903032563.
59. Al Maaitah IF, Elkenany EB. Sound velocity, electronic, optical, and mechanical properties for nano semiconductor materials (CdTe, ZnTe) under the influence of pressure. ECS J Solid State Sci Technol. 2022;11(2):023013. doi:10.1149/2162-8777/ac5578.
60. Elkenany EB. Energy band structure, acoustic velocities, optical phonon frequencies and mechanical properties of $InP_{1-x}Sb_x$ alloys under temperature and pressure. Infrared Phys Technol. 2021;115:103720. doi:10.1016/j.infrared.2021.103720.
61. Viswanathan E, Sundareswari M, Jayalakshmi DS, Manjula M, Krishnaveni S. Structural, electronic, mechanical, thermal and optical properties of $B(P, As)_{1-x}N_x$; (x = 0, 0.25, 0.5, 0.75, 1) alloys and hardness of B(P, As) under compression using DFT calculations. Indian J Phys. 2017;91(9):999–1011. doi:10.1007/s12648-017-0996-0.
62. Mukhanov VA, Kurakevych OO, Solozhenko VL. The interrelation between hardness and compressibility of substances and their structure and thermodynamic properties. J Superhard Mater. 2008;30(6):368–78. doi:10.3103/S1063457608060026.

63. Bioud N, Sun XW, Daoud S, Song T, Liu ZJ. Structural stability and thermodynamic properties of BSb under high pressure and temperature. Mater Res Express. 2018;5(8):085904. doi:10.1088/2053-1591/aad3a5.
64. Oztekin Ciftci Y, Bioud N, Kars Durukan İ. Predicting of structural, elastic, vibration, and thermodynamic properties of XThSn (X = Pt and Ni) thermoelectric materials. Phys Scr. 2025;100(1):015907. doi:10.1088/1402-4896/ad9529.
65. Fine ME, Brown LD, Marcus HL. Elastic constants vs. melting temperature in metals. Scr Metall. 1984;18(9):951–6. doi:10.1016/0036-9748(84)90267-9.
66. Varshney D, Shriya S, Varshney M, Singh N, Khenata R. Elastic and thermodynamical properties of cubic (3C) silicon carbide under high pressure and high temperature. J Theor Appl Phys. 2015;9(3):221–49. doi:10.1007/s40094-015-0183-7.
67. Chen CH, Xuan Y, Otani S. Temperature and loading time dependence of hardness of LaB_6, YB_6 and TiC single crystals. J Alloys Compd. 2003;350(1–2):L4–6. doi:10.1016/S0925-8388(02)00988-X.
68. Zagorac D, Prasad DLVK, Škundrić T, Yadav K, Singh S, Laketić S, et al. Mechanical properties and behavior of the Ti-45Nb alloy subjected to extreme conditions. CrystEngComm. 2024;26(22):2989–3004. doi:10.1039/d4ce00076e.
69. Madani MY. Study of the physical properties of the ordered SiSn alloy in the cubic zinc-blende phase [master's thesis]. Bordj Bou Arreridj, Algeria: Mohamed El-Bachir El-Ibrahimi University of Bordj Bou Arreridj; 2025.